Article

Discovery Medicine 2025; 37(193): 335–347
https://doi.org/10.24976/Discov.Med.202537193.27

Mechanisms of Age Differences in the Effectiveness of Phototherapy of Glioblastoma

Alexander Shirokov[1,2,*,†], Nikita Navolokin[2,3], Alla Bucharskaya[2,3], Inna Blokhina[2], Andrey Terskov[2], Maria Tzoy[4], Alexander Dubrovsky[4], Ivan Fedosov[4], Oxana Semyachkina-Glushkovskaya[2,*,†]

[1]Institute of Biochemistry and Physiology of Plants and Microorganisms, Russian Academy of Sciences, 410049 Saratov, Russia
[2]Department of Biology, Saratov State University, 410012 Saratov, Russia
[3]Department of Pathological Anatomy, Saratov Medical State University, 410012 Saratov, Russia
[4]Physics Department, Saratov State University, 410012 Saratov, Russia
*Correspondence: shirokov_a@ibppm.ru (Alexander Shirokov); glushkovskaya@mail.ru (Oxana Semyachkina-Glushkovskaya)
[†]These authors contributed equally.
Published: 20 February 2025

Background: Glioblastoma is an incurable and aggressive oncological disease of the brain. Recent studies have shown that transcranial non-invasive photobiomodulation is a promising new alternative method for suppression of glioblastoma growth. The lymphatic endothelium of the meningeal lymphatic vessels is an important target for the therapeutic effects of photobiomodulation. However, the functions of the meningeal lymphatic vessels decline with age. Therefore, it remains unknown whether photobiomodulation can be effective in adults and the elderly. To answer this question, this study examined the role of the meningeal lymphatic vessels and brain drainage in age-related differences in resistance to glioblastoma.

Methods: The studies were performed on 6- and 24-month-old rats using a model of fluorescent glioblastoma. Tumor progression was assessed using magnetic resonance imaging and the Fluor I *in vivo* fluorescence imaging system. Photobiomodulation was performed for 14 days for phototherapy of glioblastoma or once to study photoeffects on the brain's drainage. Brain drainage was studied by optical imaging of the lymphatic excretion of dye from the brain to the deep cervical lymph nodes, as well as by assessing the water content in brain tissues and the intracranial pressure. Histological and immunohistochemical methods were used to study apoptosis, proliferation and migration of CD8+ cells from the peripheral lymphatic system to glioblastoma.

Results: We clearly show that the network of the meningeal lymphatic vessels and brain drainage reduced in 24-month-old rats vs. 6-month-old animals ($p < 0.001$), which is accompanied by a decrease in resistance to the development of glioblastoma. Photobiomodulation significantly increases survival in 6-month-old ($p < 0.001$), but not in 24-month-old rats via an improvement of the functions of the meningeal lymphatic vessels, including a facilitating the traffic of protective CD8+ cells to glioblastoma ($p < 0.001$), reducing intracranial pressure and brain edema. The blockade of lymphatic communication between the peripheral and meningeal lymphatic systems completely suppresses the therapeutic effects of photobiomodulation in 6-month-old rats ($p < 0.001$).

Conclusion: Thus, photobiomodulation is an effective method of stimulation of brain drainage and immunity increasing resistance to glioblastoma progression in early but not in late ontogenesis due to the age-related decline in the functions of the meningeal lymphatic vessels.

Keywords: glioblastoma; photobiomodulation; aging; meningeal lymphatic vessels; brain's drainage

Introduction

Glioblastoma (GBM) is an aggressive malignancy of the brain in older adults with a very poor overall survival rate [1–3]. Age is an important factor in the incidence and survival of GBM [4]. Indeed, GBM is more common in old people with a peak in incidence between the ages of 45 and 65 years old [5]. The immune system undergoes gradual changes with aging [6,7]. Age-related reduction of lymphocytes leads to immune incompetence in the elderly resulting in increased susceptibility to infections [8]. Several studies show that immune senescence is more exaggerated in cancer subjects and is considered a worse prognosis in several solid cancers [9–11]. This age-related impaired lymphocyte function imposes a barrier to the therapy of GBM in the elderly [12,13].

Recently, transcranial non-invasive photobiomodulation (PBM) has been proposed as a promising alternative method for effective suppression of GBM progression and improvement of brain resistance to GBM [14,15]. The meningeal lymphatic vessels (MLVs), playing an important

role in the regulation of the brain's drainage, are an important target for the therapeutic effects of PBM [14,16–19]. In various models of brain diseases, including Alzheimer's disease [17,18], intraventricular hemorrhages [16], diabetes mellitus [19], and glioma [14,15], it has been established that PBM stimulates lymphatic pumping contributing to an increase in lymph flow and leading to removal of dissolved in the cerebral spinal fluid (CSF) compounds from the brain.

However, there is evidence that clearance and brain drainage are decreased with aging [20–23]. Indeed, old mice have regression in branches of the dorsal MLVs, while the basal MLVs increased in size and showed hyperplastic phenotypes that are regarded as functional adjustments to the age-related decline of CSF drainage [23,24]. These age-mediated changes in the morphology of MLVs are also associated with lymphatic valve dysfunction due to a decrease in the expression of transcription factors the prospero homeobox protein 1 (PROX1) and the forkhead box protein C2 (FOXC2) [25–28]. The basal MLVs from old mice show a dysmorphic distribution of the type IV collagen and a reduction of the number of valves compared with young mice [23]. In old mice, the lymphatic endothelial cells are dispersed, while in young animals they are elongated and distinctly clustered in the basal MLVs suggesting less lymph flow in aged MLVs [23,26,28]. The patterns of junctions in the pre-collecting lymphatic vessels in young and aged mice are quite different [27,29]. The disruption of the junctions of the lymphatic endothelial cells leading to an impaired lymph flow is considered one of the initiating factors for age-related lymphatic alterations [27,29].

Since the lymphatic endothelium of MLVs is an important target for PBM, it remains unknown whether the effects of PBM can be therapeutically effective in aged subjects in whom the MLV functions have declined. To answer this question, this study examined the effects of PBM on GBM growth in young and aged rats. To investigate the mechanisms of age-related differences in sensitivity to PBM, we studied the photo-effects on GBM cell proliferation, apoptosis, and brain drainage, including an assessment of the survival of rats with GBM after removal of the deep cervical lymph nodes (dcLNs) in 6- and 24-month-old rats.

Materials and Methods

Subjects

Wistar male rats (lot No. 2-1.2-0254P/23), aged 6 and 24 months, weighing between 380 and 597 grams, were used in all experiments. These rats were obtained from the National Laboratory Animal Resource Centre in Pushchino, Moscow, Russia. The animal experiments were conducted in accordance with the «Guide for the Care and Use of Laboratory Animals», the Directive 2010/63/EU on the Protection of Animals Used for Scientific Purposes, and the guidelines provided by the Ministry of Science and Higher Education of the Russian Federation (№ 742 from 13.11.1984). Additionally, the experimental protocols were approved by the Bioethics Commission of the Saratov State University (Protocol No. 8, 18.04.2023). The choice of rat age is related to the evaluation of PBM efficacy in young (6 months old) and in aged animals (24 months old), corresponding to 25–30 and 65–75 years of age in humans [30]. The experiments were performed in the following groups: (1) the control included 6-month-old rats without PBM; (2) 6-month-old rats + PBM; (3) the control included 24-month-old rats without PBM; (4) 24-month-old rats + PBM; n = 5–10 in each group in all experiments.

Model of GBM

The C6 rat glioma cell line (lot No. 101) was obtained from the Russian Cell Culture Collection of Vertebrates, which is part of the Institute of Cytology at the Russian Academy of Sciences in Saint Petersburg, Russia. To create a fluorescent model of glioblastoma, we prepared a transfected C6-TurboRFP cell line as described in this publication [14]. C6 cells were cultured in a growth medium called Dulbecco's Modified Eagle Medium (DMEM) (C410E; Paneco, Moscow, Russia), which was supplemented with 2.5% fetal bovine serum (FB-1101/500; Biosera, Cholet, France), 4 mM glutamine (F031; Paneco, Moscow, Russia), penicillin (50 IU/mL), and streptomycin (50 mg/mL) (A066; Paneco, Moscow, Russia). The C6 rat glioma cells were transfected with TurboRFP-C DNA plasmids (FP231; Eurogen, Moscow, Russia) using the method of liposomal transfection with Lipofectamine 2000 Transfection Reagent (11668019; Invitrogen, Waltham, MA, USA). After transfection, the cells were selected using a geneticin G418 antibiotic (ant-gn-1; InvivoGen, Toulouse, France). The control of bacterial and fungal contamination and the determination of the morphology of C6 cells were carried out using immunofluorescence microscopy (Leica DMI3000 B, Leica Microsystems, Wetzlar, Germany) with DAPI (4′,6-Diamidino-2-phenylindole) and Hoechst Nucleic Acid Stains (D1306; Invitrogen, Waltham, MA, USA). The C6 cell morphology was stable. For additional control of mycoplasma contamination, PCR testing was performed with Mycoplasma Detection Kit (PP-401L, Jena Bioscience, Jena, Germany). The resulting cell line, C6-TurboRFP, has a negative mycoplasma test, and stable cultural and morphological characteristics.

Subsequently, C6 glioma cells were genetically modified with C6—TurboRFP-C DNA constructs. The C6—TurboRFP cells, at a concentration of 5×10^5 cells per rat, were injected into the brain at the following coordinates: AP—1 mm, ML—1 mm, DV—4 mm, with a volume of 15 µL. GBM volume was monitored by magnetic resonance imagining (MRI) using the Clin scan 7T tomograph (Bruker, Mannheim, Germany). The fluorescence imaging system Fluor I *in vivo* (NeoScience Co., Ltd., Suwon, Korea) was used to visualize the C6-TurboRFP cells

in the isolated brains (excitation-500–550 n, and emission-550–650 nm). Using the NEOimage version 1.0.1 software (NeoScience Co., Ltd., Suwon, Korea), the fluorescent RFP signal was separated from the background and illumination caused by autofluorescence and reflected light.

The Kaplan-Meier method is used to analyze 'time-to-event' data to compare survival between the two groups. Log Rank and chi-square were used [31]. The survival rate was expressed as a percentage and calculated as the ratio of the number of deceased rats to the total number of animals at the start of the experiment, multiplied by 100. The two survival curves were compared using a statistical test called the log-rank test. This test is used to test the null hypothesis that there is no difference between the two survival curves. The significance of the differences was further assessed using the χ^2 test [32]. The statistical analysis of survival was carried out through a specialized automated program IBM SPSS Statistics 26.0.0 (IBM, Chicago, IL, USA).

Magnetic Resonance Imaging (MRI) of GBM

GBM volume was assessed using the Clin scan 7T tomograph (Bruker, Mannheim, Germany) as previously described [33]. Briefly, rats were anesthetized with 2% isoflurane at 1 L/min N_2O/O_2—70/30 ratio. The anatomical T2-weighted magnetic resonance imaging scans were obtained using a rapid acquisition with relaxation enhancement (RARE) sequence. The parameters were as follows: repetition time (TR) of 5000 milliseconds, echo time (TE) of 56 milliseconds, field of view (FOV) of 4 centimeters by 4 centimeters, slice thickness of 1 millimeter, slice gap of 1.1 millimeters, and 12 slices. The matrix size was 256 by 256, and the number of averages was three. The T1-weighted imaging was performed using the RARE technique with a TE of 9.6 milliseconds, a TR of 1000 milliseconds, and a RARE factor of 2, resulting in four averages. This process took 4 minutes and 16 seconds to assess the tumor volumes. The regions of visible hyperenhancement in each slice were outlined on the T2-weighted and corresponding T1-weighted images using NIH ImageJ (Bethesda, MD, USA), v.2.9.0, open-source image processing software. The volumes were then calculated using MATLAB software version 2018b (The MathWorks, Inc., Natick, MA, USA). For data analysis, GraphPad Prizm v.6.0 (GraphPad Software, Inc., San Diego, CA, USA) was used.

PBM of GBM

A 1050 nm light-emitting diodes (LEDs) in pulse mode were used for PBM. The head plate with LEDs fixed on the shaved head of a rat using dental acrylic (Zhermack SpA, Badia Polesine, Italia) under inhalation anesthesia with 1% isoflurane (Sigma-Aldrich, St Luis, MO, USA, at the rate of 1 L/min N_2O/O_2—70/30 ratio). PBM was carried out during 61 min: 17 min—light, 5 min—pause, 17 min—light, 5 min—pause, 17 min—light as previously described in the following publications [14,15]. The irradiation dose was 30 J/cm^2 for a single application (for the study of CSF-drainage) and 0.42 kJ/cm^2 for 14 days PBM course of GBM therapy that was performed daily in rats with 4-week-old GBM. The temperature on the surface of the brain remained unchanged after PBM (The light intensity at the skull does not exceed 0.5 W/cm^2), which is in line with our previous research findings [15]. To monitor the temperature on the brain surface before and during PBM, we employed a type-A-K3 thermocouple (Ellab, Hillerød, Denmark) and a flexible thermocouple probe (IT-23, 0.23 mm diameter, Physitemp Instruments LLC, Clifton, NJ, USA), which was inserted between the parietal bone and the brain into the epidural space.

Optical Monitoring of CSF Drainage

Optical studies of brain drainage involve the introduction of dyes into CSF and subsequent observation of the removal of dye from brain tissues to the periphery. Therefore, in our studies we injected the fluorescein isothiocyanate (FITC)-dextran (2% fluorescein isothiocyanate-dextran (FITCD), 7 µL, Sigma, St Louis, MO, USA) into the right lateral ventricle (AP—1.0 mm; ML—1.4 mm; DV—3.5 mm) via polyethylene catheter (PE-10, 0.28 mm ID × 0.61 mm OD, Scientific Commodities Inc., Lake Havasu City, Arizona, USA). 1.5 hours after the injection, the removal of FITCD from the brain to dcLNs was monitored using confocal microscopy (Nikon A1R MP, Nikon In struments Inc., Melville, LA, USA). The implantation of a chronic catheter into the right lateral ventricle was performed according to the protocol published by Devos and Miller [34]. For image processing was used a Fiji open-source platform for biological image analysis (Fiji Is Just ImageJ, ImageJ2 14.0/1.54g; Java 1.8.0_332 [64 bit]) [35].

Histological, Immunohistochemical and Confocal Analysis

The rats were euthanized using a CO_2 chamber (Threeshine Inc., Yuseong-gu, Daejeon, Korea). The brains and lymph nodes were removed and preserved in a 10% formalin solution. The tissue samples were then prepared for paraffin embedding and subjected to standard immunohistochemistry procedures. The paraffin sections were stained with hematoxylin and eosin, and immunohistochemistry was performed using the REVEAL Polyvalent HRP-DAB Detection System. Monoclonal antibodies were used at a dilution of 1:100, including Bcl-2-Associated X protein (Bax) (ab216985, Abcam, Waltham, MA, USA), Ki67 (clone SP6, ab16667, Abcam, Waltham, MA, USA), p53 (ab131442, Abcam, Waltham, MA, USA), and CD95 (FNab03016, FineTest, Wuhan, China). Secondary antibodies were used at a dilution of 1:500, and were labeled with horseradish peroxidase. The percentage of positive cells in 10 fields of view for each sample was calculated

using a MicroVisor medical transmitted light µVizo-103 (LOMO, St Petersburg, Russia) with a magnification of 774.

For confocal imaging, the brains and dcLNs were fixed at 4% buffered formalin and were sliced with a thickness of 40–50 microns using a vibratome (Leica, Wetzlar, Germany). Afterward, sections were processed according to the standard immunohistochemistry (IHC) protocol with primary antibodies (rat anti-CD8+ antibody (1:500; ab22378, Abcam, Waltham, MA, USA), mouse anti-neural/glial antigen 2 (NG2) antibody (1:500; ab50009, Abcam, Waltham, MA, USA) and rabbit anti-lymphatic vessel endothelial hyaluronan receptor 1 (LYVE-1) antibody (1:500; ab10278, Abcam, Waltham, MA, USA) and second antibodies (goat anti-rat IgG (H+L) Alexa Fluor 488 (ab150157, Abcam, Waltham, MA, USA), goat anti-mouse IgG (H+L) Alexa Fluor 594 (ab150116, Abcam, Waltham, MA, USA) and goat anti-rabbit IgG (H+L) Alexa Fluor 555 (ab150078, Abcam, Waltham, MA, USA). Before confocal microscopy (Nikon A1R MP, Nikon Instruments Inc., Melville, LA, USA), 15 µL of mounting liquid (50% glycerin in the phosphate buffered saline with the DAPI at a concentration of 2 µg/mL) was applied to the section. DAPI, Alexa Fluor 488, and Alexa Fluor 555 were excited at wavelengths of 405, 488, and 561 nanometers, respectively. Evans blue was excited at 647 nanometers. Three-dimensional data was collected by acquiring images in the x, y, and z planes. Images were acquired using NIS-Elements 6.14 software (Nikon Instruments Inc., Melville, LA, USA) and analyzed using Fiji open source platform for biological image analysis (Fiji Is Just ImageJ, ImageJ2 14.0/1.54, Java 1.8.0 332 [64 bit]) and Vaa3D 3.4.3 open-source visualization and analysis software.

Measurement of Brain Water Content

Brain water content was determined by the wet-dry weight ratio method as described previously [36,37]. Rats (n = 10/group) were sacrificed by decapitation. The brains were removed immediately and cut into small pieces. Brains were weighed on an analytical balance (Denver Instrument Co., Bohemia, NY, USA) to obtain the wet weight and then dried at 100 °C for 48 h to obtain the dry weight. Afterward, they dried at 100 °C for 48 h to obtain the dry weight. Brain water content was expressed as (wet weight – dry weight)/wet weight of brain tissue × 100%.

Measurement of Intracranial Pressure (ICP)

ICP was monitored via a catheter (PE-50) filled with artificial CSF (BioChemazone, Ontario, Canada) inserted into the right lateral ventricle and connected to the pressure transducer TSD104A with a DA100C amplifier (Biopac Systems, Inc., Goleta, CA, USA). The recording of ICP was performed using a Biopac MP160 data acquisition system and AcqKnowledge software 5.0.5. (Biopac Systems, Inc., Goleta, CA, USA).

Statistical Analysis

Microsoft Office Excel and SPSS Statistics Base 17.0 (IBM, New York, NY, USA) for Windows were used for statistical analysis. The Shapiro-Wilk test was used to find out whether the parameter values in the groups followed a normal distribution. If the Shapiro-Wilk test showed that the distribution of a parameter departed from normality ($p < 0.05$), a non-parametric Wilcoxon test and Mann-Whitney test were used for calculation of the median (Me), 25th and 75th percentiles Q (25–75), maximum and minimum. Using this method, median differences were determined at $Z \geq 1.96$ at a significance level of $p < 0.05$ (with more than 95% probability). If the Shapiro-Wilk test did not show evidence of non-normality, we decided to use parametric tests. The results are presented as mean ± standard error of the mean (SEM). Differences from the initial level in the same group were evaluated with Welch's *t*-test and analysis of variance (ANOVA)-2 (post hoc analysis with Duncan's rank test) to determine whether differences existed among the means of three or more groups. Welch's *t*-test consists of the division of the difference between the arithmetic means of two (control and experimental) samples by the natural estimate of the mean-square deviation of this. $T \geq 1.96$ indicates a 95% probability of the mean values being different with this method. The significance levels were set at $p < 0.05$ for the whole analysis.

Results

Age Differences in the PBM-Therapy of GBM: Photo-Effects on CSF Drainage

In the first step, we studied the PBM effects on resistance to GBM progression in 6- and 24-month-old rats by assessing the GBM volume and survival. Fig. 1a,b illustrate fluorescent imaging of the glioma growth pattern with tumor invasion onto the dorsal surface of the brain in some animals from both age groups. The MRI data revealed that the GBM volume was lower in young rats compared to adult animals (233 ± 2.2 mm^3 vs. 262 ± 9.5 mm^3, $p < 0.001$ between 6- and 24-month-old rats, n = 10 in each group) (Fig. 1c). Slower growth of GBM in 6-month-old rats was accompanied by higher survival rates compared to 24-month-old animals (χ^2 test = 3.677, $p = 0.05$, n = 8 in each group) (Fig. 1e). PBM significantly reduced the GBM volume (133 ± 11.2 mm^3 vs. 233 ± 2.2 mm^3, $p <$ 0001 between 6-month-old rats with and without the PBM course; 269 ± 4.7 mm^3 vs. 262 ± 9.5 mm^3, ns between 24-month-old rats with and without the PBM course, n = 10 in each group) (Fig. 1c). Fig. 1a,b also demonstrate that after the PBM course in 6-month-old rats, no glioma growth onto the brain surface was observed due to a decrease in its size, while in 24-month-old rats, the glioma growth pattern did not change. Furthermore, PBM increased survival in 6-month-old but not in 24-month-old rats (χ^2 test = 22.610, p

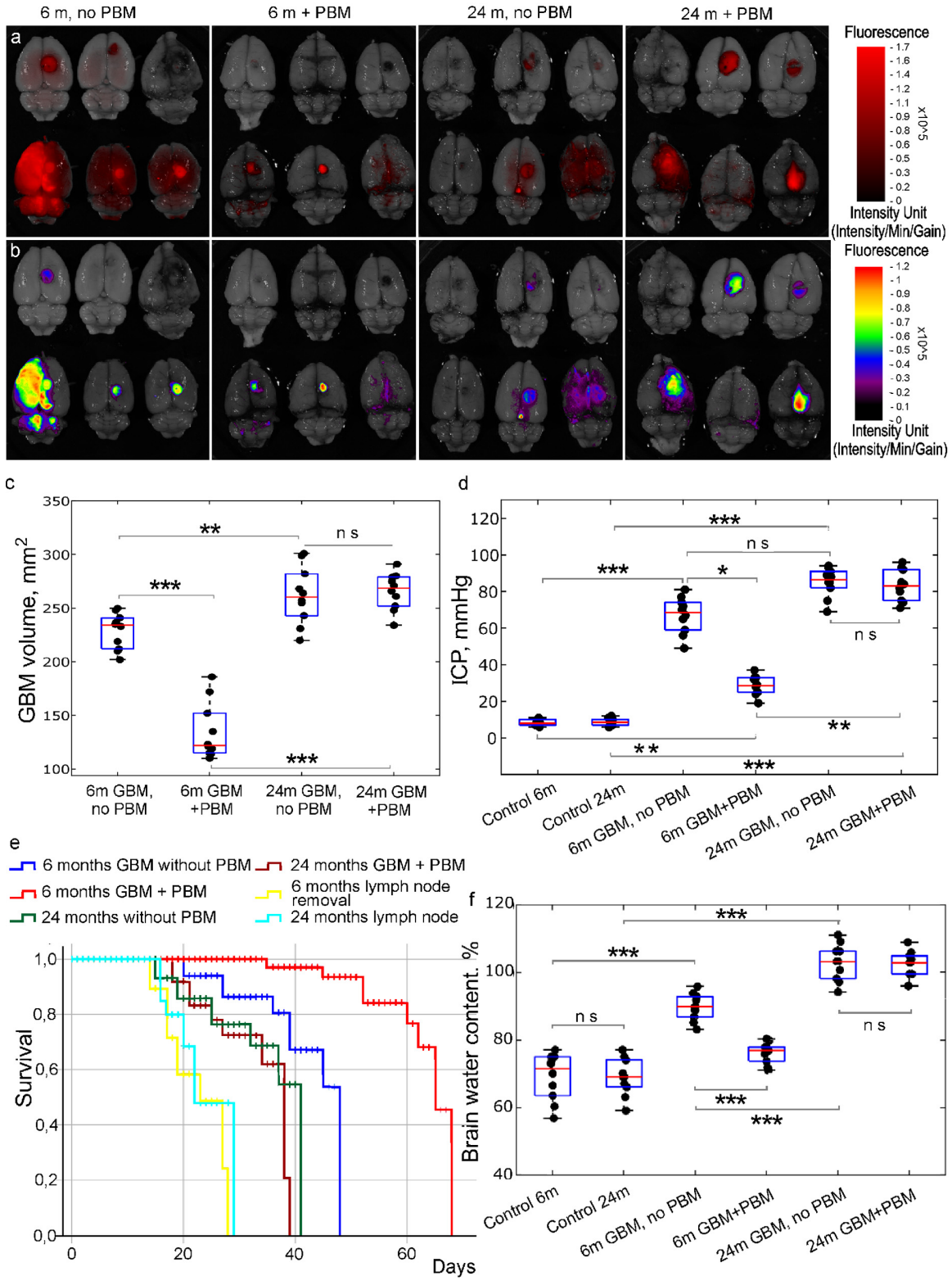

Fig. 1. The PBM effects on the GBM progression, survival rate and brain drainage in young and adult rats. (a,b) Fluorescent imaging of GBM size in 6- and 24-month-old rats without PBM and after PBM with red scale (a) and rainbow scale (b) fluorescence intensity (n = 6 in each group); (c,d,f) the MRI analysis of glioma size (c), ICP (d) and brain water content (f) in the tested groups; (e) Kaplan-Meier overall survival plots in the tested groups without and after PBM; in (c–f) n = 10, the ANOVA test with the post hoc Duncan test, *, $p < 0.05$; **, $p < 0.01$; ***, $p < 0.001$; ns, not significant. PBM, photobiomodulation; GBM, glioblastoma; MRI, magnetic resonance imagining; ICP, intracranial pressure; ANOVA, analysis of variance.

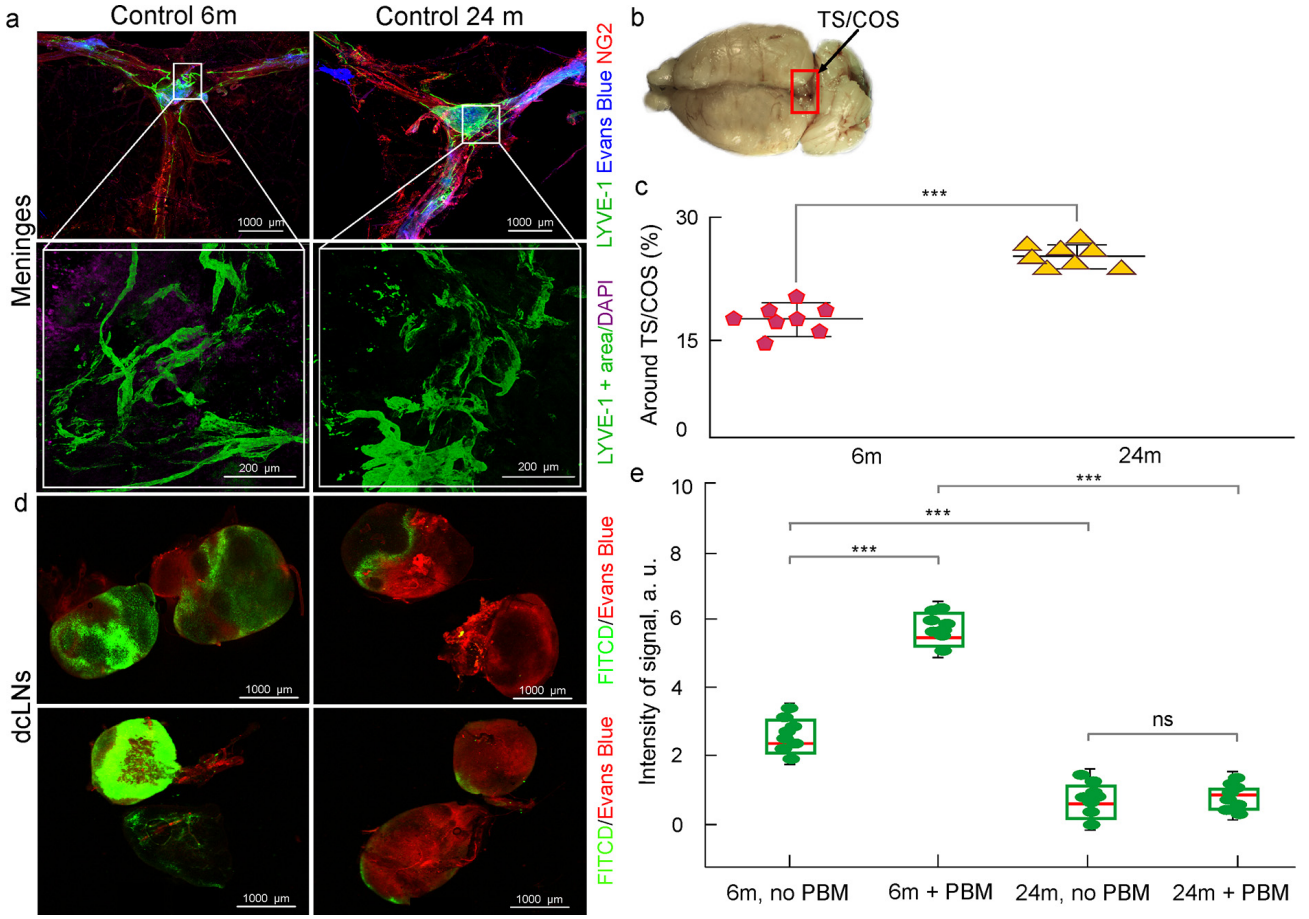

Fig. 2. Age differences in the MLV network and the PBM effects on lymphatic removal of FITCD from the brain of healthy rats. (a) Representative images of the lymphatic vessel endothelial hyaluronan receptor 1 (LYVE-1) + vessels (green) covering the main venous sinuses (TS/COS) in 6- and 24-month-old rats. The blood vessels are filled with Evans Blue (blue) and labeled with NG2 (red); (b) the schematic illustration of ROI for the confocal analysis of MLVs; (c) quantitative analysis of LYVE-1 coverage expressed in % of ROI; (d) representative images of dcLNs in 6- and 24-month-old healthy rats before and after PBM (single application); (e) quantitative analysis of FITCD in 6- and 24-month-old healthy rats before and after PBM, n = 8 in each group, ***, $p < 0.001$, the ANOVA test with the post hoc Duncan test. ns, not significant. MLV, meningeal lymphatic vessel; FITCD, fluorescein isothiocyanate (FITC)-dextran; TS, transverse sinus; COS, confluence of sinuses.

= 0.001 between 6-month-old rats without and after PBM; χ^2 test = 0.706, ns between 24-month-old rats with and without PBM, n = 8 in each group) (Fig. 1e).

A reduced CSF drainage and an increased ICP due to excessive fluid accumulation in the brain are important factors in GBM progression [38]. Therefore, in the next step, we studied changes in ICP and brain water content during GBM growth, as well as the effects of PBM on these parameters in rats of different ages with GBM. Fig. 1d,f show that 6-month-old rats demonstrated lower GBM-induced ICP and brain water content than 24-month-old animals (ICP: 59.5 ± 7.1 mmHg vs. 90.5 ± 6.9 mmHg, $p < 0.001$ between 6- and 24-month-old rats; brain water: 88.4 ± 5.4% vs. 104.3 ± 5.8%, $p < 0.01$ between 6- and 24-month-old rats, n = 10 in each group). Notably, PBM improved these parameters of CSF drainage in young but not in adult rats (ICP: 27.3 ± 3.0 mmHg vs. 59.5 ± 7.1 mmHg, $p < 0.001$ between 6-month-old rats with and without PBM and 89.8 ± 2.3 mmHg vs. 90.5 ± 6.9 mmHg, not significant (ns) between 24-month-old rats with and without PBM; brain water: 76.2 ± 2.8% vs. 88.4 ± 5.4%, $p < 0.05$ between 6-month-old rats with and without PBM and 103.0 ± 4.6 vs. 104.3 ± 5.8, ns between 24-month-old rats with and without PBM, n = 10 in each group) (Fig. 1d,f). There were no differences in ICP and brain water content in healthy rats from the two age groups (ICP: 8.3 ± 1.4 mmHg vs. 9.1 ± 1.9 mmHg, ns between 6- and 24-month-old rats; brain water: 72.1 ± 9.8% vs. 69.9 ± 4.9%, ns between 6- and 24-month-old rats, n = 10 in each group) (Fig. 1d,f).

Thus, PBM improves resistance to GBM development in 6-month-old but not in 24-month-old rats through stimulating effects on CSF drainage, which are manifested in a decrease in ICP and in water accumulation in brain tissues.

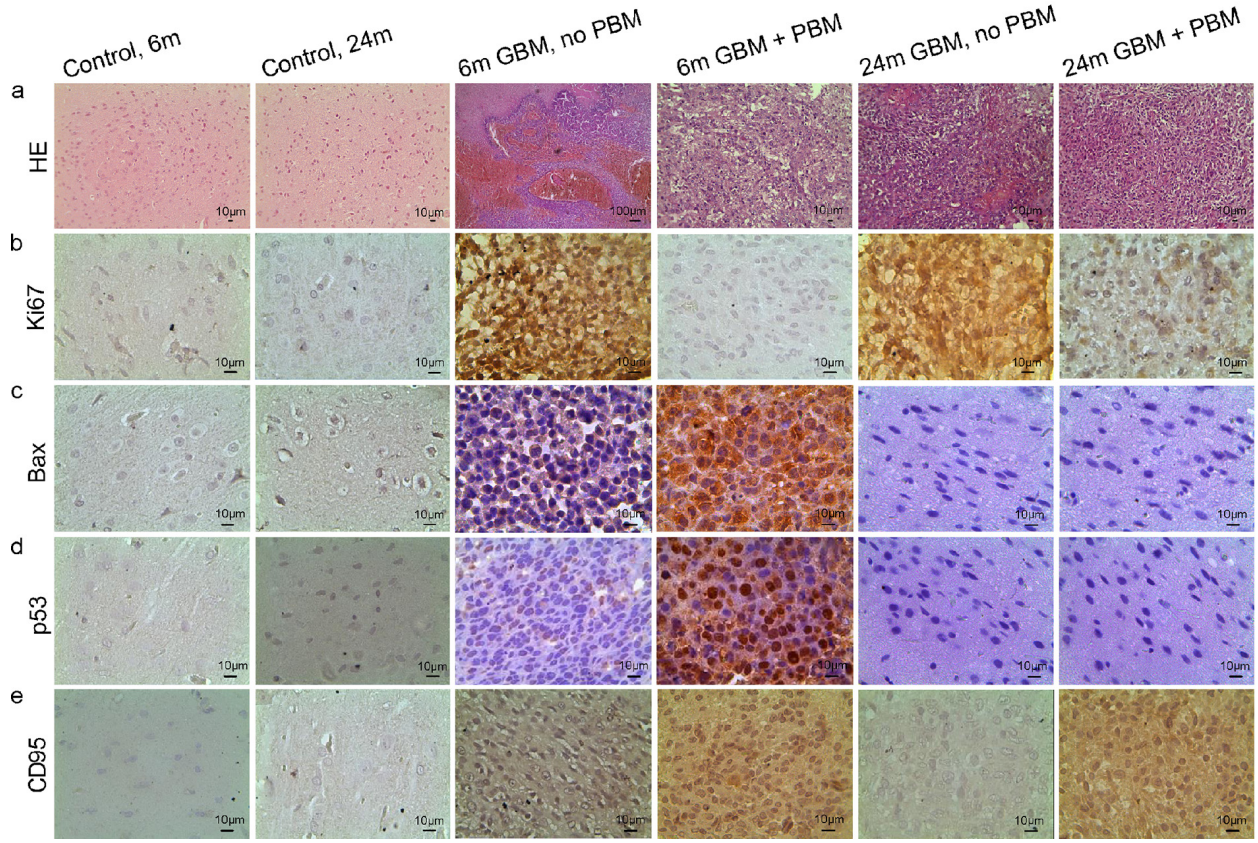

Fig. 3. Age differences in the PBM effects on proliferation and apoptosis of GBM cells. (a) Representative images of the staining hematoxylin and eosin (H&E) analysis of brain tissues from the tested groups, including 6- and 24-month-old healthy rats, rats with GBM without and after PBM; (b–e) representative images of the immunohistochemistry (IHC) analysis of the expression of markers of proliferation (Ki67, (b)) of GBM cells as well as intrinsic (Bcl-2-Associated X protein (Bax), P53, (c,d)) and extrinsic (CD95, (e)) apoptosis. The quantitative analysis of immunopositive cells (shown in brown) expressing Ki67, Bax, p53 and CD95 is presented in Table 1.

Age Differences in the Stimulating PBM Effects on Lymphatic Removal of FITCD: the Role of the MLV Network

To answer the question what is the role of brain drainage in resistance to GBM development, we studied the survival of rats with GBM after removal of dcLNs, which are the first anatomical station for CSF collection [39]. Fig. 1e illustrates that before the blockade of CSF outflow from the brain, young rats were more resistant to the GBM development than adult ones (χ^2 test = 3.677, p = 0.05 between 6- and 24-month-old rats before removal of dcLNs; n = 8 in each group), after removal of dcLNs, mortality in 6-month-old rats increased sharply (χ^2 test = 24.161, p = 0.001 between 6-month-old rats before and after removal of dcLNs), which equalized their chances of survival vs. 24-month-old rats (χ^2 test = 0.791, ns between 6- and 24-month-old rats after removal of dcLNs, n = 8 in each group). The survival among adult animals also decreased after the removal of dcLNs (χ^2 test = 6.249, p = 0.01 between 24-month-old rats before and after removal of dcLNs, n = 8 in each group).

Since MLVs play a key role in CSF drainage [16–23,40,41], we hypothesized that a higher survival rate in 6-month-old rats compared to 24-month-old animals might be due to age-related differences in the MLV network. To address this question, we evaluated the LYVE-1 + vessels covered the main venous sinuses (the transverse sinus (TS) and the confluence of sinuses (COS)) as well as lymphatic removal of FITCD from the right lateral ventricle in healthy rats of both ages (Fig. 2a,b). Fig. 2a,c clearly show that there were more LYVE-1 + vessels in 24-month-old rats than in 6-month-old animals (25.925 ± 0.66 a.u vs. 17.15 ± 0.6 a.u., $p < 0.001$, n = 8 in each group). However, lymphatic removal of FITCD was decreased in adult rats compared with young ones suggesting CSF reduction in healthy 24- vs. 6-month-old rats (0.68 ± 0.16 a.u. vs. 2.675 ± 0.18 a.u., $p < 0.001$ between 6- and 24-month-old rats, n = 8 in each group) (Fig. 2d,e). These facts, which at first glance seem contradictory, explain the results presented in Fig. 2a. Despite the fact that the representation of the LIVE-1 + vessels is higher in 24-month-old rats around TS/COS, we observed lymphatic hyperplasia in adult animals that are

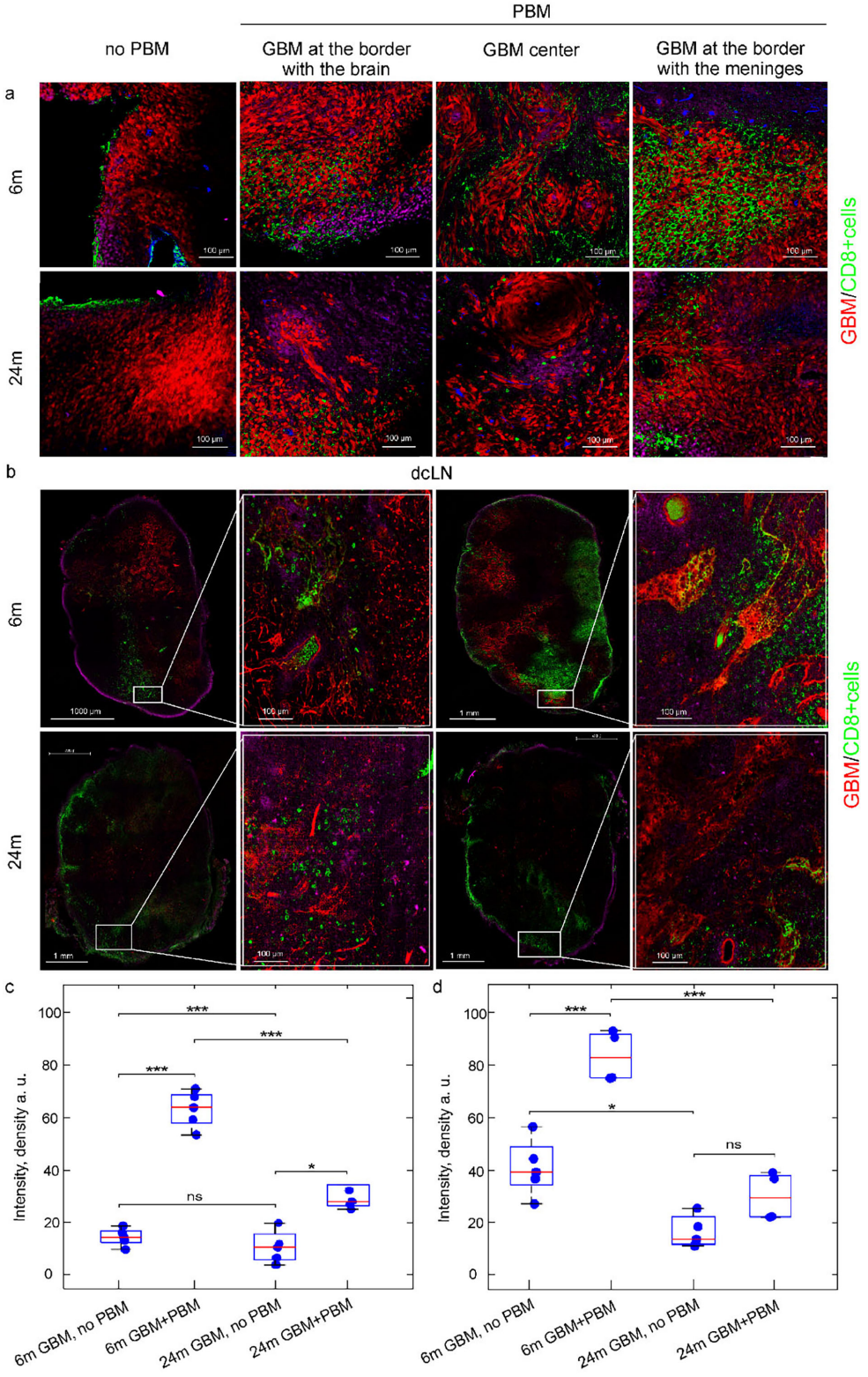

Fig. 4. Age differences in the PBM effects on the brain immune response to the GBM growth. (a) Representative images of the CD8+ T cells presence in the GBM center and border as well as in the meninges in 6- and 24-month-old rats without and after PBM. (b) Representative images of the CD8+ T cells presence in deep cervical lymph nodes (dcLNs) in 6- and 24-month-old rats without and after PBM. The magnified images show the results of maximum intensity projection on a Z-stack of 10-15 focal planes in depth. (c,d) Quantitative analysis of the intensity of the fluorescent signal from the CD8+ T cells in GBM center (c) and in dcLN (d); n = 5 in each group, *, $p < 0.05$; ***, $p < 0.001$, the ANOVA test with the post hoc Duncan test. ns, not significant.

Table 1. The expression of markers of proliferation and apoptosis (%).

Markers	6 m	24 m	6 m GBM, no PBM	6 m GBM + PBM	24 m GBM, no PBM	24 m GBM + PBM
Ki67	-	-	60.7 ± 8.1	11.43 ± 2.44 †††	90.31 ± 4.40 ***	78.02 ± 9.35 ***
Bax	-	-	10.01 ± 1.2	73.23 ± 6.10 †††	-	-
p53	-	-	19.12 ± 2.5	51.08 ± 3.93 †††	-	-
CD95	-	-	-	95.51 ± 1.21	-	62.22 ± 4.00 ***

***, $p < 0.001$ between age groups; †††, $p < 0.001$ between GBM without and after PBM; n = 8 in each group; the Welch's t test.

considered as an indicator of reduced CSF drainage [23]. This fact is supported by the results of photostimulation of MLVs, which showed an increase in the lymphatic excretion of FITCD from the brain to dcLNs only in 6-month-old rats and the absence of such effects in 24-month-old animals (5.8 ± 0.15 a.u. vs. 2.675 ± 0.18 a.u., $p < 0.001$ between 6-month-old rats with and without PBM, 0.425 ± 0.07 a.u. vs. 0.68 ± 0.16 a.u., ns between 24-month-old rats with and without PBM, n = 8 in each group) (Fig. 2e).

The results of this series of experiments clearly show that age-related changes in MLVs and CSF drainage may be the cause of attenuated resistance to the GBM development and sensitivity to PBM in 24- vs. 6-month-old rats.

Age Differences in the PBM Effects on Proliferation and Apoptosis of GBM Cells

The histological analysis revealed that in both age groups without PBM, GBM was represented by tumor tissue with extensive hemorrhages and necrosis. The tumor contours were not clear. Furthermore, high cell density in the field of view and mitoses were found in tumor cells (Fig. 3a). After PBM, in both age groups, GBM had clearer boundaries with brain tissue, the tumor was more localized, there were no hemorrhages, GBM cells were located more sparsely and had dystrophic damage. The mitoses were not detected in GBM cells (Fig. 3a).

The IHC analysis revealed the high expression of a marker of proliferation Ki67 in rats with GBM that was more pronounced in 24-month-old rats vs. 6-month-old animals (Table 1, Fig. 3b). Expression of intrinsic apoptosis markers (Bax and P53) was weakly expressed in 6-month-old rats with GBM and was absent in 24-month-old rats (Fig. 3c,d). In young rats with GBM, PBM significantly suppressed the expression of Ki67 which was associated with an increase in intrinsic and additional stimulation of extrinsic pathways of apoptosis (Table 1, Fig. 3b–e). In contrast to young rats, in adult rats, PBM had weak effects on the Ki67 expression and stimulated only intrinsic apoptosis (CD95) (Table 1, Fig. 3b–e).

These results indicate age-related differences in the molecular mechanisms of the therapeutic effects of PBM, which are most effective in young rats and weakly manifested in adult animals.

Age Differences in the PBM Effects on Immune Response to GBM Growth

The cytotoxic CD8+ T cell infiltration is a crucial mechanism responsible for maintaining resistance to GBM progression [42]. The activated CD8+ T cells by infiltrating into the tumor stimulate in GBM cells the apoptosis providing suppression of tumor growth [39,43,44]. However, GBM is characterized by the limitation of CD8+ T cells in the tumor region [45,46]. This immune suppression is associated with peritumoral edema preventing the migration of CD8+ T cells and the lack of signaling molecules for activation of its generation in the cervical lymph nodes [46].

Since PBM was found to increase CSF drainage, the effects of PBM on the immune response to GBM growth were studied by assessing the presence of CD8+ T cells in the tumor. Fig. 4a,c clearly demonstrates that without PBM, the CD8+ T cells were found only at GBM border, while after PBM, the number of CD8+ T cells in the tumor center and, especially in the meninges increased significantly in 6-month-old rats and weakly in 24-month-old animals (63.4 ± 4.2 vs. 15 ± 2.5, $p < 0.001$ between 6-month-old rats with and without PBM; 27.3 ± 2.0 vs. 10.7 ± 5.1, $p < 0.05$ between 24-month-old rats with and without PBM, n = 5 in each group). Similar therapeutic dynamics were observed in the lymph nodes, where the number of CD8+ T cells increased by PBM, which was more pronounced in young rats compared to adult animals (84.9 ± 1.8 vs. 39.9 ± 8.9, $p < 0.001$ between 6-month-old rats with and without PBM; 32.2 ± 1.6 vs. 15.6 ± 2.3, $p < 0.05$ between 24-month-old rats with and without PBM, n = 5 in each group) (Fig. 4b,d). These results indicate more effective photostimulation of immune response in 6-month-old rats than in 24-month-old animals.

Discussion

This study investigated the role of MLVs in age differences in resistance to GBM and sensitivity to the therapeutic effects of PBM. The results revealed that GBM size and survival were higher in 6-month-old rats compared to 24-month-old animals. These data are consistent with the fact that GBM is more common in the elderly [5]. The decrease in the MLV functions may be one of the reasons explaining age-related differences in resistance to GBM development. Indeed, our results revealed that 24-month-old rats exhibited lymphatic hyperplasia, which is manifested by the proliferation of the lymphatic endothelium. Lymphatic

hyperplasia is regarded as a compensatory mechanism responsible for functional adjustments to a decline in tissue drainage [24]. Ahn *et al*. [23] confirmed that the hyperplastic basal MLVs in aged rodents are associated with reduced CSF drainage. They found that lymphatic hyperplasia is accompanied by lymphatic valve dysfunction in adult mice, which has also been established in other studies [24,26–29]. The basal MLVs in old rodents are characterized by a dysmorphic distribution of type IV collagen and fewer lymphatic valves compared with the basal MLVs in young animals [24]. The expression of transcription factors that are essential for the maintenance of the lymphatic valves, such as PROX1 and FOXC2, is reduced with age [23,25–27]. Ahn *et al*. [23] clearly demonstrate that in young rodents, lymphatic cells in the valves of the basal MLVs are elongated and distinctly clustered, while in adult animals they are dispersed suggesting that the aged basal MLVs encounter less lymph flow. Indeed, our results showed a decrease in brain drainage in 24-month-old rats compared to 6-month-old animals, which was determined by a lower intensity of FITCD excretion from the brain to dcLNs in old vs. young rodents.

Age-related decline in the MLV function leading to a decrease in CSF drainage was accompanied by greater fluid accumulation in brain tissues and higher ICP growth in 24- vs. 6-month-old rats with GBM. The lymphatic endothelium of MLVs is a target for the therapeutic effects of PBM [16–19]. In our previous studies on young mice and rats, it was found that PBM stimulates contractility of the lymphatic vessels and increases lymph flow in them, leading to an increase in drainage and removal of CSF-dissolved compounds from brain tissues [16–19]. Since 24-month-old rats showed morphological changes in MLVs, which was accompanied by a decrease in their functions, adult rats were insensitive to phototherapy of GBM. Thus, in 6-month-old rats with GBM, PBM effectively improved water content in brain tissues and ICP, while in 24-month-old animals such effects were absent.

There is emerging evidence that MLVs and associated with them cervical lymphatics play an important role in the regulation of immune responses to the GBM growth [14,15,42,47–49]. It is discussed that stimulation of the MLV functions and brain drainage may represent an advance in suppressing brain tumor growth [14,15,42,47–49]. Indeed, our data showed that the preservation of the MLV functions in 6-month-old rats with GBM was accompanied by internal apoptosis in GBM cells, which was completely absent in 24-month-old rats. The level of GBM cell proliferation was lower in young rats compared to adult animals. At the same time, PBM significantly increased internal and additionally activated external apoptosis, which was accompanied by an effective decrease in GBM cell proliferation in 6-month-old rats. Unlike young rats, in adult animals, PBM stimulated only internal apoptosis and weakly reduced GBM cell proliferation.

By stimulating the brain's drainage, PBM improves the migration of protective CD8+ leukocytes from the cervical lymph nodes to GBM tissue [15]. We assumed that effective brain drainage contributes to the optimization of immune responses against GBM due to improvements in the microenvironment of the tumor and compensation of CSF outflow. Indeed, despite the fact that the CD8+ T cells were detected exclusively at the tumor margins in rats of both ages, the number of these cells in dcLNs was greater in 6- vs. 24-month-old rats. Note that PBM significantly improved migration of the tumor-infiltrating cytotoxic CD8+ T cells to GBM center in young, but not in adult rats. Our results indicating a CD8+ protective leukocyte deficiency in GBM tissue before PBM are consistent with data from other researchers [45,46]. There is strong evidence that increased proliferative activity of the CD8+ T cells associated with a suppression of the Ki67 expression is a favorable prognostic factor for survival in patients with cancer [50]. This is explained by the fact that the CD8+ T cells produce antitumor antibodies supporting antitumor immune responses [42,51].

The lack of desired photo effects on immune responses in 24-month-old animals may also be explained by a decrease in immunoreactivity with age. The immune system undergoes gradual decline with aging leading to a decrease in the production of lymphocytes and accordingly to impaired capacity of the immune system to react to foreign antigens [6,7]. This age-related impaired lymphocyte function imposes a barrier to the therapy of GBM in the elderly [12,13].

Thus, the preservation of the MLV functions in 6-month-old rats compared to 24-month-old animals is accompanied by their higher survival rate and resistance to the GBM progression, as well as higher sensitivity to photostimulating effects on lymphatic drainage and protective immune responses of the brain.

Our studies of age differences in resistance to the GBM progression and sensitivity to PBM are limited to using rats of only two ages (6 and 24 months of age). Taking into account the gradual decrease in the MLV functions with age and their important role in the resistance to the development of GBM, the study of the correlation between age-related changes in the MLV functions and the effectiveness of photo-therapy of GBM will significantly expand the understanding of the mechanisms of PBM at different stages of ontogenesis. The effectiveness of the therapeutic effects of PBM is increased during sleep due to the night activation of the brain's drainage [15,18,52,53]. Since aged rats are not sensitive to the PBM effect on GBM, it is logical to assume that the use of PBM in sleeping aged rats may partially increase the therapeutic effects of PBM in this age group, which requires further research.

Conclusions

In sum, the results of this study clearly demonstrate that the aging brain is accompanied by a decline of the MLV functions leading to a reduction of CSF drainage. These age-related changes are associated with a decrease in resistance to GBM development and sensitivity to the therapeutic effects of PBM in 24- vs. 6-month-old rats. Indeed, PBM effectively stimulates the excretion of excess fluid only from the brain of young rats with GBM leading to a decrease in ICP. These therapeutic effects of PBM significantly increase survival and protective immune responses to GBM development in young rats but not in adult animals. Thus, PBM might be a promising and non-invasive method for suppression of GBM growth by photo-stimulation of the MLV functions that is significantly limited in the aging brain.

Abbreviations

COS, confluence of sinuses; CSF, cerebral spinal fluid; DAPI, 4′,6-Diamidino-2-phenylindole; dcLNs, deep cervical lymph nodes; FOXC2, forkhead box protein C2; FITCD, fluorescein isothiocyanate (FITC)-dextran; GBM, glioblastoma; LEDs, light-emitting diodes; LYVE-1, lymphatic vessel endothelial hyaluronan receptor 1; MLVs, meningeal lymphatic vessels; MRI, magnetic resonance imaging; ns, not significant; PBM, photobiomodulation; PROX1, prospero homeobox protein 1; TS, transverse sinus.

Availability of Data and Materials

The data that support the findings of this study are available on request from the corresponding authors.

Author Contributions

Conceptualization, OSG, AS; methodology, AS, IB, AB; software, IF; validation and formal analysis, MT; investigation, NN, AB, IB; resources, AS; data curation, AS, OSG, IF; writing—original draft preparation, OSG and AS; writing—review and editing, OSG; visualization, AT, AD; supervision, OSG; project administration, OSG. NN, AT, MT, and AD have made significant contributions to the development of the concept and design, data collection, analysis and interpretation. All authors contributed significantly to editorial changes of important content. All authors read and approved the final manuscript. All authors have participated sufficiently in the work and agreed to be accountable for all aspects of the work.

Ethics Approval and Consent to Participate

All experimental procedures were performed in accordance with the «Guide for the Care and Use of Laboratory Animals», the Directive 2010/63/EU on the Protection of Animals Used for Scientific Purposes, and the guidelines from the Ministry of Science and High Education of the Russian Federation (№ 742 from 13.11.1984), which have been approved by the Bioethics Commission of the Saratov State University (Protocol No. 8, 18.04.2023).

Acknowledgment

We thank center for the collective use of scientific equipment «Simbioz» and immunochemistry laboratory IBPPM RAS (Russian Federation, Saratov) for their support with the immunofluorescence analysis and confocal microscopy within the current research project (Project No. GR 1022040700963-8).

We thank the “Technoinfo” company (Russian Federation, Moscow), who provided the fluorescence imaging system Fluor I *in vivo* and members of the Laboratory “Remotely controlled systems for Theranostics” of the Scientific Medical Center of the Saratov State University, Lomova M.V. and Kalinova A.E. for their support with fluorescence imaging of C6-RFP mouse brain tumor.

We thank the students for their assistance in conducting the experiments: Viktoria Adushkina, Daria Zlatogosrkaya, Arina Evsyukova, Alexander Dubrovsky, Alexander Dmitrenko, Matvey Tuzhilkin, Inna Elizarova, Valeria Krupnova, Maria Manzhaeva and for the development of computer programs for data analysis: Timophey Inozemcev, Dmitry Myagkov, Dmitry Tuktarov, Sergey Popov, Anastasiia Semiachkina-Glushkovskaia, Egor Ilyukov.

Funding

This research was supported by a grant from the Russian Science Foundation 23-25-00296.

Conflict of Interest

The authors declare no conflict of interest.

References

[1] Alhalaseh YN, Abdulelah ZA, Abu-Shanab A, Armouti AO, Amarin JZ, Mansour R, *et al*. Glioblastoma in adolescents and young adults: An age-based comparative study from Jordan over a 17-year period. Cancer Epidemiology. 2021; 73: 101948.

[2] Miller KD, Ostrom QT, Kruchko C, Patil N, Tihan T, Cioffi G, *et al*. Brain and other central nervous system tumor statistics, 2021. CA: a Cancer Journal for Clinicians. 2021; 71: 381–406.

[3] Stupp R, Taillibert S, Kanner A, Read W, Steinberg D, Lhermitte B, *et al*. Effect of Tumor-Treating Fields Plus Maintenance Temozolomide vs Maintenance Temozolomide Alone on Survival in Patients With Glioblastoma: A Randomized Clinical Trial. JAMA. 2017; 318: 2306–2316.

[4] Lin Z, Yang R, Li K, Yi G, Li Z, Guo J, *et al*. Establishment of age group classification for risk stratification in glioma patients. BMC Neurology. 2020; 20: 310.

[5] Wang GM, Cioffi G, Patil N, Waite KA, Lanese R, Ostrom QT, *et al*. Importance of the intersection of age and sex to under-

stand variation in incidence and survival for primary malignant gliomas. Neuro-oncology. 2022; 24: 302–310.

[6] Aiello A, Farzaneh F, Candore G, Caruso C, Davinelli S, Gambino CM, *et al*. Immunosenescence and Its Hallmarks: How to Oppose Aging Strategically? A Review of Potential Options for Therapeutic Intervention. Frontiers in Immunology. 2019; 10: 2247.

[7] Huff WX, Bam M, Shireman JM, Kwon JH, Song L, Newman S, *et al*. Aging- and Tumor-Mediated Increase in $CD8^{+}CD28^{-}$ T Cells Might Impose a Strong Barrier to Success of Immunotherapy in Glioblastoma. ImmunoHorizons. 2021; 5: 395–409.

[8] Mou D, Espinosa J, Lo DJ, Kirk AD. CD28 negative T cells: is their loss our gain? American Journal of Transplantation: Official Journal of the American Society of Transplantation and the American Society of Transplant Surgeons. 2014; 14: 2460–2466.

[9] Falci C, Gianesin K, Sergi G, Giunco S, De Ronch I, Valpione S, *et al*. Immune senescence and cancer in elderly patients: results from an exploratory study. Experimental Gerontology. 2013; 48: 1436–1442.

[10] Giunco S, Petrara MR, Bergamo F, Del Bianco P, Zanchetta M, Carmona F, *et al*. Immune senescence and immune activation in elderly colorectal cancer patients. Aging. 2019; 11: 3864–3875.

[11] Montes CL, Chapoval AI, Nelson J, Orhue V, Zhang X, Schulze DH, *et al*. Tumor-induced senescent T cells with suppressor function: a potential form of tumor immune evasion. Cancer Research. 2008; 68: 870–879.

[12] Fülöp T, Montgomery RR. Editorial overview: Immune senescence: known knowns and unknown unknowns. Current Opinion in Immunology. 2014; 29: vii–ix.

[13] Kanesvaran R, Cordoba R, Maggiore R. Immunotherapy in Older Adults With Advanced Cancers: Implications for Clinical Decision-Making and Future Research. American Society of Clinical Oncology Educational Book. American Society of Clinical Oncology. Annual Meeting. 2018; 38: 400–414.

[14] Semyachkina-Glushkovskaya O, Sokolovski S, Fedosov I, Shirokov A, Navolokin N, Bucharskaya A, *et al*. Transcranial Photosensitizer-Free Laser Treatment of Glioblastoma in Rat Brain. International Journal of Molecular Sciences. 2023; 24: 13696.

[15] Shirokov A, Blokhina I, Fedosov I, Ilyukov E, Terskov A, Myagkov D, *et al*. Different Effects of Phototherapy for Rat Glioma during Sleep and Wakefulness. Biomedicines. 2024; 12: 262.

[16] Li D, Liu S, Yu T, Liu Z, Sun S, Bragin D, *et al*. Photostimulation of brain lymphatics in male newborn and adult rodents for therapy of intraventricular hemorrhage. Nature Communications. 2023; 14: 6104.

[17] Li D, Lin H, Sun S, Liu S, Liu Z, He Y, *et al*. Photostimulation of lymphatic clearance of β-amyloid from mouse brain: a new strategy for the therapy of Alzheimer's disease. Frontiers of Optoelectronics. 2023; 16: 45.

[18] Blokina I, Iluykov E, Myagkov D, Tuktarov D, Popov S, Inozemzev T, *et al*. Photobiomodulation under Electroencephalographic Controls of Sleep for Stimulation of Lymphatic Removal of Toxins from Mouse Brain. Journal of Visualized Experiments: JoVE. 2024.

[19] Liu S, Li D, Yu T, Zhu J, Semyachkina-Glushkovskaya O, Zhu D. Transcranial photobiomodulation improves insulin therapy in diabetic microglial reactivity and the brain drainage system. Communications Biology. 2023; 6: 1239.

[20] Da Mesquita S, Louveau A, Vaccari A, Smirnov I, Cornelison RC, Kingsmore KM, *et al*. Functional aspects of meningeal lymphatics in ageing and Alzheimer's disease. Nature. 2018; 560: 185–191.

[21] Tarasoff-Conway JM, Carare RO, Osorio RS, Glodzik L, Butler T, Fieremans E, *et al*. Clearance systems in the brain-implications for Alzheimer disease. Nature Reviews. Neurology. 2015; 11: 457–470.

[22] Ma Q, Ineichen BV, Detmar M, Proulx ST. Outflow of cerebrospinal fluid is predominantly through lymphatic vessels and is reduced in aged mice. Nature Communications. 2017; 8: 1434.

[23] Ahn JH, Cho H, Kim JH, Kim SH, Ham JS, Park I, *et al*. Meningeal lymphatic vessels at the skull base drain cerebrospinal fluid. Nature. 2019; 572: 62–66.

[24] Gousopoulos E, Proulx ST, Scholl J, Uecker M, Detmar M. Prominent Lymphatic Vessel Hyperplasia with Progressive Dysfunction and Distinct Immune Cell Infiltration in Lymphedema. The American Journal of Pathology. 2016; 186: 2193–2203.

[25] Cho H, Kim J, Ahn JH, Hong YK, Mäkinen T, Lim DS, *et al*. YAP and TAZ Negatively Regulate Prox1 During Developmental and Pathologic Lymphangiogenesis. Circulation Research. 2019; 124: 225–242.

[26] Sabine A, Agalarov Y, Maby-El Hajjami H, Jaquet M, Hägerling R, Pollmann C, *et al*. Mechanotransduction, PROX1, and FOXC2 cooperate to control connexin37 and calcineurin during lymphatic-valve formation. Developmental Cell. 2012; 22: 430–445.

[27] Sabine A, Bovay E, Demir CS, Kimura W, Jaquet M, Agalarov Y, *et al*. FOXC2 and fluid shear stress stabilize postnatal lymphatic vasculature. The Journal of Clinical Investigation. 2015; 125: 3861–3877.

[28] Sweet DT, Jiménez JM, Chang J, Hess PR, Mericko-Ishizuka P, Fu J, *et al*. Lymph flow regulates collecting lymphatic vessel maturation in vivo. The Journal of Clinical Investigation. 2015; 125: 2995–3007.

[29] Zolla V, Nizamutdinova IT, Scharf B, Clement CC, Maejima D, Akl T, *et al*. Aging-related anatomical and biochemical changes in lymphatic collectors impair lymph transport, fluid homeostasis, and pathogen clearance. Aging Cell. 2015; 14: 582–594.

[30] Ghasemi A, Jeddi S, Kashfi K. The laboratory rat: Age and body weight matter. EXCLI Journal. 2021; 20: 1431–1445.

[31] Kaplan EL, Meier P. Nonparametric estimation from incomplete observations. Journal of the American Statistical Association. 1958; 53: 457–481.

[32] Bewick V, Cheek L, Ball J. Statistics review 12: survival analysis. Critical Care (London, England). 2004; 8: 389–394.

[33] Bragin DE, Kameneva MV, Bragina OA, Thomson S, Statom GL, Lara DA, *et al*. Rheological effects of drag-reducing polymers improve cerebral blood flow and oxygenation after traumatic brain injury in rats. Journal of Cerebral Blood Flow and Metabolism: Official Journal of the International Society of Cerebral Blood Flow and Metabolism. 2017; 37: 762–775.

[34] DeVos SL, Miller TM. Direct intraventricular delivery of drugs to the rodent central nervous system. Journal of Visualized Experiments: JoVE. 2013; e50326.

[35] Schindelin J, Arganda-Carreras I, Frise E, Kaynig V, Longair M, Pietzsch T, *et al*. Fiji: an open-source platform for biological-image analysis. Nature Methods. 2012; 9: 676–682.

[36] Wang J, Tsirka SE. Neuroprotection by inhibition of matrix metalloproteinases in a mouse model of intracerebral haemorrhage. Brain: a Journal of Neurology. 2005; 128: 1622–1633.

[37] Zhu W, Gao Y, Chang CF, Wan JR, Zhu SS, Wang J. Mouse models of intracerebral hemorrhage in ventricle, cortex, and hippocampus by injections of autologous blood or collagenase. PloS One. 2014; 9: e97423.

[38] Qin X, Liu R, Akter F, Qin L, Xie Q, Li Y, *et al*. Peri-tumoral brain edema associated with glioblastoma correlates with tumor recurrence. Journal of Cancer. 2021; 12: 2073–2082.

[39] Philip M, Schietinger A. $CD8^{+}$ T cell differentiation and dysfunction in cancer. Nature Reviews. Immunology. 2022; 22:

209–223.

[40] Louveau A, Smirnov I, Keyes TJ, Eccles JD, Rouhani SJ, Peske JD, *et al*. Structural and functional features of central nervous system lymphatic vessels. Nature. 2015; 523: 337–341.

[41] Ma Q, Schlegel F, Bachmann SB, Schneider H, Decker Y, Rudin M, *et al*. Lymphatic outflow of cerebrospinal fluid is reduced in glioma. Scientific Reports. 2019; 9: 14815.

[42] Mauldin IS, Jo J, Wages NA, Yogendran LV, Mahmutovic A, Young SJ, *et al*. Proliferating CD8$^+$ T Cell Infiltrates Are Associated with Improved Survival in Glioblastoma. Cells. 2021; 10: 3378.

[43] Ferrantelli F, Manfredi F, Chiozzini C, Leone P, Giovannelli A, Olivetta E, *et al*. Long-Term Antitumor CD8$^+$ T Cell Immunity Induced by Endogenously Engineered Extracellular Vesicles. Cancers. 2021; 13: 2263.

[44] Raskov H, Orhan A, Christensen JP, Gögenur I. Cytotoxic CD8$^+$ T cells in cancer and cancer immunotherapy. British Journal of Cancer. 2021; 124: 359–367.

[45] Waldman AD, Fritz JM, Lenardo MJ. A guide to cancer immunotherapy: from T cell basic science to clinical practice. Nature Reviews. Immunology. 2020; 20: 651–668.

[46] Xia A, Zhang Y, Xu J, Yin T, Lu XJ. T Cell Dysfunction in Cancer Immunity and Immunotherapy. Frontiers in Immunology. 2019; 10: 1719.

[47] Steele MM, Jaiswal A, Delclaux I, Dryg ID, Murugan D, Femel J, *et al*. T cell egress via lymphatic vessels is tuned by antigen encounter and limits tumor control. Nature Immunology. 2023; 24: 664–675.

[48] Hu X, Deng Q, Ma L, Li Q, Chen Y, Liao Y, *et al*. Meningeal lymphatic vessels regulate brain tumor drainage and immunity. Cell Research. 2020; 30: 229–243.

[49] Song E, Mao T, Dong H, Boisserand LSB, Antila S, Bosenberg M, *et al*. VEGF-C-driven lymphatic drainage enables immunosurveillance of brain tumours. Nature. 2020; 577: 689–694.

[50] Nakano O, Sato M, Naito Y, Suzuki K, Orikasa S, Aizawa M, *et al*. Proliferative activity of intratumoral CD8(+) T-lymphocytes as a prognostic factor in human renal cell carcinoma: clinicopathologic demonstration of antitumor immunity. Cancer Research. 2001; 61: 5132–5136.

[51] Xie Q, Ding J, Chen Y. Role of CD8$^+$ T lymphocyte cells: Interplay with stromal cells in tumor microenvironment. Acta Pharmaceutica Sinica. B. 2021; 11: 1365–1378.

[52] Xie L, Kang H, Xu Q, Chen MJ, Liao Y, Thiyagarajan M, *et al*. Sleep drives metabolite clearance from the adult brain. Science (New York, N.Y.). 2013; 342: 373–377.

[53] Fultz NE, Bonmassar G, Setsompop K, Stickgold RA, Rosen BR, Polimeni JR, *et al*. Coupled electrophysiological, hemodynamic, and cerebrospinal fluid oscillations in human sleep. Science (New York, N.Y.). 2019; 366: 628–631.